Ocean Engineering 147 (2018) 659–675

Contents lists available at ScienceDirect

Ocean Engineering

journal homepage: www.elsevier.com/locate/oceaneng

Comparison of different approaches tracking a wing-tip vortex

D.-F. Feder [a,*], M. Dhone [b], N. Kornev [b], M. Abdel-Maksoud [a]

[a] Hamburg University of Technology (TUHH), Institute for Fluid Dynamics and Ship Theory, Am Schwarzenberg-Campus 4 (C), 21073 Hamburg, Germany
[b] University of Rostock, Chair of Modelling and Simulation, Albert-Einstein-Straße 2, 18059 Rostock, Germany

ARTICLE INFO

Keywords:
Tip vortex
Grid free vortex method
Turbulence modelling
Adaptive mesh refinement
Adaptive vorticity confinement

ABSTRACT

This paper compares the performance of different grid based and grid free modelling approaches to predict the tip vortex evolution in both near and far wing wake fields. The grid based methods cover different turbulence modelling approaches, adaptive mesh refinement and the adaptive vorticity confinement (VC) method using the OpenFOAM code. Computational vortex method (CVM) coupled with the OpenFOAM simulation of the near field is utilised to properly predict the tip vortex behaviour in the far field. All simulation results are compared to results of the wind tunnel experiments conducted by Devenport et al. (1996). The comparison is based on the analysis of the vortex core parameters: the core size, the peak tangential velocity and the axial velocity deficit. Additionally, the results are compared with another numerical study by Wells (2009, 2010). It turns out that turbulence modelling plays an important role since simple one and two-equation models overpredict the turbulence intensity in the vortex core resulting in its fast decay. The potential of the adaptive VC method depends on the underlying turbulence model. Grid free vortex method shows a good potential to improve the simulation accuracy.

1. Introduction

Wing-tip vortices decay slowly and extend far downstream in the wake. Strong tip vortices with a large lifetime can be observed in many engineering applications with (rotating) lifting surfaces. In marine engineering the most important application is the marine propeller hydrodynamics. In case of submerged ship propellers tip vortex cavitation may create noise and lead to erosion of the rudder. The noise prediction is of big importance because it disturbs animals like whales and reduces comfort of people on board ship. The propeller slipstream including the tip vortices prescribes the flow at the rudder and therewith influences the rudder forces. Lifting foils are used in shipbuilding to damp ship roll motions and for the creation of the dynamic lift on hydrofoil ships. In these cases the trailing tip vortices may influence the inflow of the propeller or foils moving downstream in the wake. A further important area where tip vortices play a dominant role is the wake of aircraft. The evolution of the tip vortices of landing and starting aircraft has been extensively studied with respect to the hazard of wake encounter by other craft flying close to the big one. Also for Wing-in-Ground (WIG) effect vehicles the wake and tip vortex evolution has a strong influence on the flight stability (see e.g. Kornev and Matveev (2003), Rozhdestvensky (2006)).

The prediction of tip vortices with computational fluid dynamics (CFD) is a challenge as inherent artificial dissipation effects lead to an unphysically strong decay of the vortices. The artificial dissipation or numerical diffusion results from numerical errors due to the discretisation and turbulence modelling. Feder and Abdel-Maksoud (2016b) provide further information on this topic in conjunction with the numerical prediction of tip vortices. An accurate numerical prediction of the tip vortex evolution is limited by a huge amount of necessary computational resources and imperfection of available mathematical models.

Several numerical and experimental studies deal with the evolution of tip vortices and the difficulties concerning their prediction. Gerz, Holzäpfel and Misaka worked extensively on the numerical prediction of tip vortices within the wake of aircraft, see e.g. Gerz et al. (2002), Holzäpfel et al. (2003), Misaka et al. (2013) and Stephan et al. (2014) or Chow et al. (1994). Their approach is usually based on the application of large eddy simulations (LES) targeting to predict the vortex decay of aircraft including the influence of the ground effect on the tip vortices and their evolution in the atmospheric boundary layer.

Several studies deal with the analysis of tip vortex evolution in the near field, so up to a few chord lengths downstream. An interesting study is published by Samal et al. (2013) who investigated the flow structure of a wing-tip vortex behind a sweptback and tapered NACA 0015 wing at

* Corresponding author.
E-mail addresses: dag.feder@tuhh.de (D.-F. Feder), mahesh.dhone2@uni-rostock.de (M. Dhone), nikolai.kornev@uni-rostock.de (N. Kornev), m.abdel-maksoud@tuhh.de (M. Abdel-Maksoud).

https://doi.org/10.1016/j.oceaneng.2017.09.036
Received 20 December 2016; Received in revised form 22 August 2017; Accepted 24 September 2017
Available online 27 October 2017

$Re = 181000$. Their simulation results showed a good agreement with experimental results. Further studies by Nash'at et al. (2013) have been conducted to analyse the wake in the near field of a NACA 0012 wing. This paper focuses on grid based and grid free methods to capture the details of vortices especially further downstream after the vortex has rolled up and started to decay. Kornev and Abbas (2016) studied CFD performance to predict the near vortex field in the wake of an oscillating wing at distances of one and half chords from the trailing edge. They showed a good agreement with experimental results of Birch and Lee (2005).

Experimental investigations of wing-tip vortices in wind tunnels confirm that tip vortices extend for long distances in the wake. Devenport et al. (1996) carried out an extensive study of a tip vortex trailing from a NACA 0012 wing until 30 chord lengths downstream of the wing. They present experimental data of turbulence properties as well as the tangential and axial velocities in the vicinity of the vortex core. The quality of the experimental data is superior to many other investigations because they were corrected for the wandering of the tip vortex core caused by instability of wind tunnel flow and possible wing vibration. Wells published a numerical study for the Devenport test case and analysed the performance of different turbulence models (see Wells (2009); Wells et al. (2010)). In the near field, the accuracy of the simulation results using a Reynolds stress turbulence model is very good. Further downstream, Wells observes excessive diffusion of the tip vortex which is not supported by experimental results. Within this study, different grid based and grid free simulation approaches are validated for prediction of the tip vortex evolution using the Devenport test case.

According to the measurements of Devenport et al. (1996) the flow in the vicinity of the vortex core is laminar. Utilisation of standard Reynolds-averaged Navier-Stokes (RANS) turbulence models based on Boussinesq approach leads to an overprediction of the turbulence viscosity within the vortex core which in turn results in its increased decay rate. As a remedy of this disadvantage, several improved turbulence models, validated in this paper, were proposed by different authors: curvature corrections for RANS models, hybrid RANS-LES methods and Reynolds stress transport models. The artificial numerical viscosity can be reduced by adaptive mesh refinement (AMR) and the adaptive vorticity confinement (VC) methods which are also in the focus of this paper. The first approach refines the mesh in the vicinity of the vortex core and the second approach introduces a momentum source term which should counteract the numerical diffusion. The VC method was developed by Steinhoff and colleagues in 1992 (Steinhoff et al. (1992), Steinhoff and Underhill (1994) and Steinhoff et al. (2005)) and further developed by several authors. It overcomes the significant deficiency of the previous VC formulations as it lacks the necessity of a user-defined forcing coefficient. Recent applications of the VC method showed its potential for ship propeller hydrodynamics, see e.g. Zhang et al. (2014). Another work to be mentioned here is presented by O'Regan et al (see O'Regan et al. (2016)). who demonstrated that the potential of VC is larger in conjunction with LES turbulence modelling than with any URANS approach. This behaviour was observed also by Feder and Abdel-Maksoud in Feder and Abdel-Maksoud (2016a) for the adaptive VC method.

2. Test case

This study targets to validate CFD models using the benchmark test case thoroughly studied in wind tunnel measurements presented in Devenport et al. (1996). The basic setup of the experiment is shown in Fig. 1. During the experiment, the evolution of a tip vortex generated by a rectangular wing with the NACA 0012 profile was studied. The wing with a blunt tip has the following dimensions: a span of 0.879 m and a chord length of $c = 0.203$ m. The wind tunnel has a quadratic test section of 1.83 m width and 7.33 m length.

Devenport et al. provide the most extensive data for the Reynolds number $Re = 530000$ (based on the chord length) and for 5° angle of attack. There, the vortex is tracked downstream until 30 chord lengths behind the leading edge of the wing. Experimental data are provided for axial and tangential velocity profiles through the vortex core and for turbulence properties (e.g. the turbulent kinetic energy). The target of the simulation approaches used in this paper is to predict the evolution of tip vortices until large distances downstream. For this purpose the test case of Devenport et al. is more informative than other experiments at which the tip vortices are tracked only in the near wake of wings.

Besides, another advantage of this wind tunnel data is the proper correction for the vortex wandering motion. This slow side-to-side movement is usually observed for wind tunnel generated tip vortices. Without a proper correction of this effect, the experimental data would suggest an increased vortex decay. The way how the experimental data is corrected is presented in details in Devenport et al. (1996). Feder and Abdel-Maksoud (2016b) did not observe wandering within a similar previous numerical study. This observation was based on the Hexpress mesh with 6.0 M cells and the SA-DDES turbulence model. The solver settings were equal to the ones used for the transient simulations within this study. As no wandering was observed within the simulations, the corresponding correction is not necessary. The postprocessing of the simulation results will be presented in Section 4.1.

3. Numerical setup

The simulations are conducted with OpenFOAM (see Weller et al. (1998)) on grids with hexahedral cells generated with Hexpress and structured grids generated with ANSYS ICEM CFD. The coordinate system is set according to Devenport et al. (1996) and displayed in Fig. 2a. The origin is placed at the leading edge on the wing-tip. The x-axis points downstream and the y-axis points along the wing. The computational domain is shown in Fig. 2a. The inlet boundary is located at $x/c = -7.4$ whereas the outlet at $x/c = 46.7$. The boundaries with y- and z-normals denote the walls of the wind tunnel's test section. The size of the domain's cross section corresponds to the measuring section of the wind tunnel and the location of the wing in the cross section is identical to the experimental one.

3.1. Grids

3.1.1. Hexpress low Re number grid

The low Reynolds number mesh was generated with Hexpress version 5.1 (the turbulent boundary layer is well resolved up to the viscous sublayer). Fig. 2a shows the (medium) mesh at certain boundaries.

An advantage of the Hexpress mesh is the possibility to attain a homogeneous cell size with a desired refinement level in the vicinity of the vortex core. The cell size around the tip vortex in the measurement section ($x/c = [5, 30]$) is chosen to obtain about eight cells inside the mean measured core diameter. The total cell number is approximately 6.0 M. Since the first cell height is small 2×10^{-5} m which yields $Y^+ \approx 1$, no wall functions are applied within the simulation. A few cell (about 20) layers are used within the boundary layer.

This mesh was also used within the previous studies by Feder and

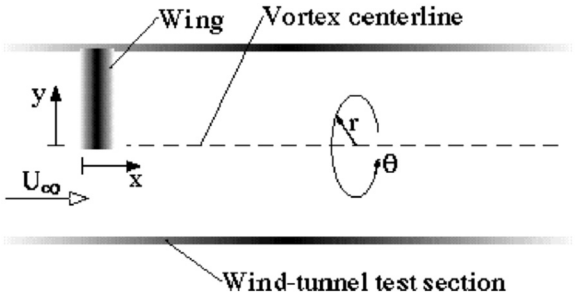

Fig. 1. Schematic view of the wind tunnel test section, from Devenport et al. (1996).

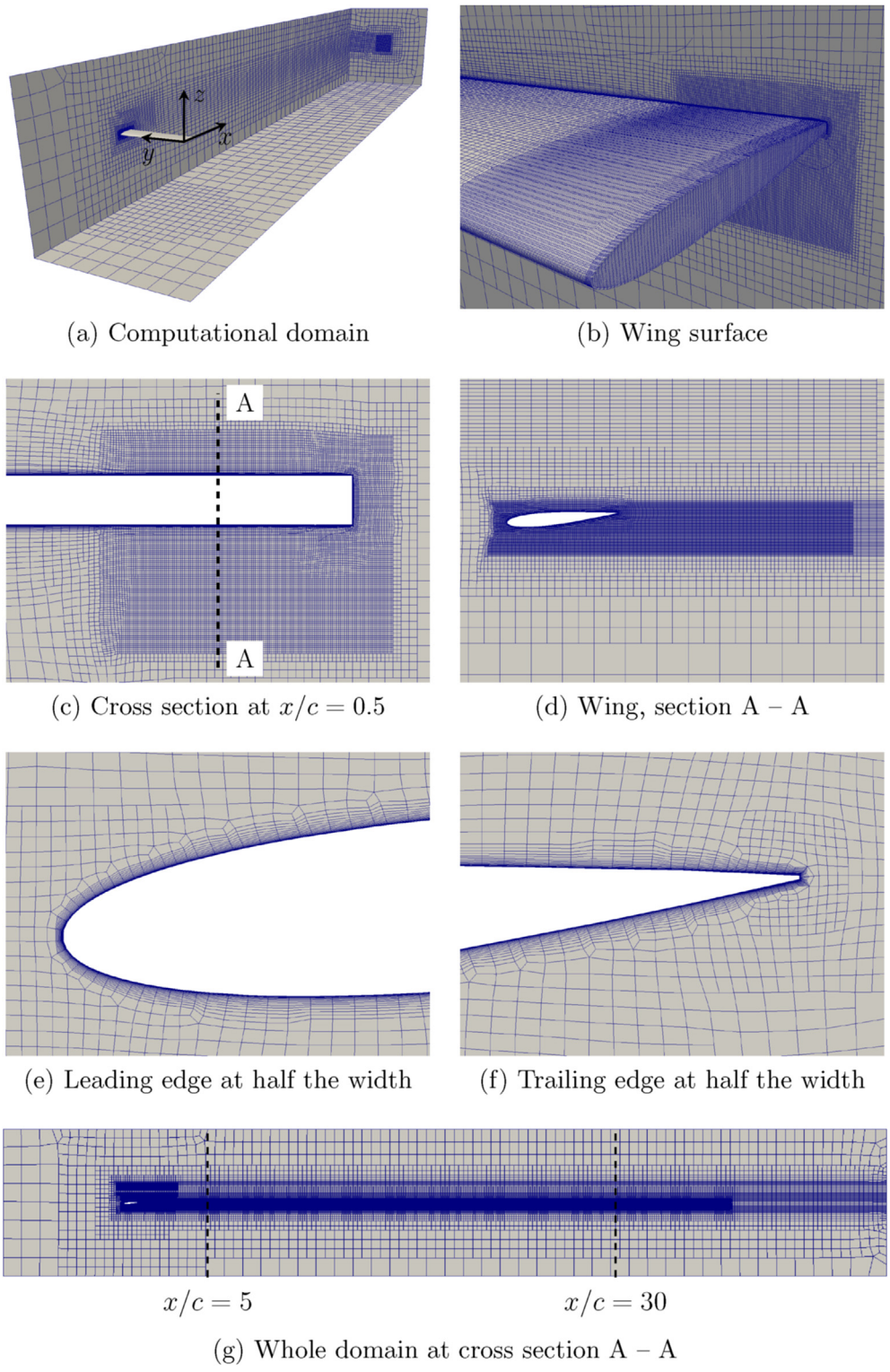

(a) Computational domain (b) Wing surface

(c) Cross section at $x/c = 0.5$ (d) Wing, section A – A

(e) Leading edge at half the width (f) Trailing edge at half the width

(g) Whole domain at cross section A – A

Fig. 2. Computational domain and mesh views.

Abdel-Maksoud on the Devenport test case. There, the influence of (static) mesh refinement was investigated.

3.1.2. *ICEM high Re number grid*

Three meshes of different resolutions are generated in ANSYS ICEM CFD. The first mesh with 2.7 million of cells is initially coarse in the whole computational domain, while gets a little finer in the regions close to the wing (see Fig. 3). By the use of the special routine of OpenFoam, two boxes are introduced for static refinement within the vortex core. The first box extends from the leading edge to $x/c = 10$ distance, while the second one extends further to $x/c = 20$. In all the three directions each cell in the first box is refined with the factor of two, while this factor in the second box is four. This results in intermediate fine 7.2 million mesh grid. Further refining the 7.2 million mesh in both boxes by doubling the cell number in all three directions results in the finest mesh of 42.2 million cells (see Fig. 4). The non dimensional position of the first

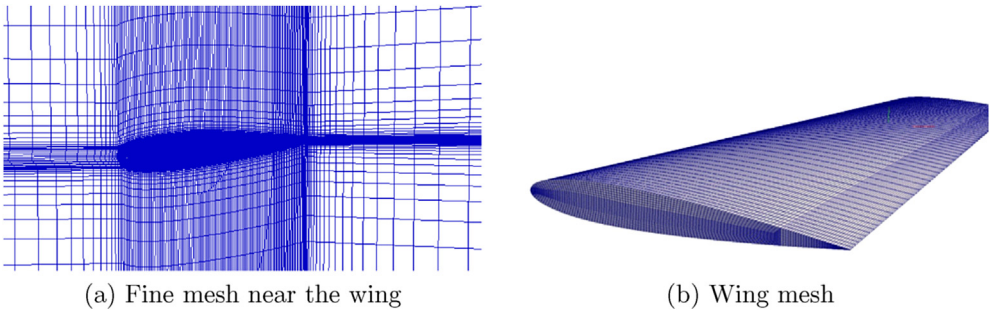

Fig. 3. 2.7 million mesh (coarse).

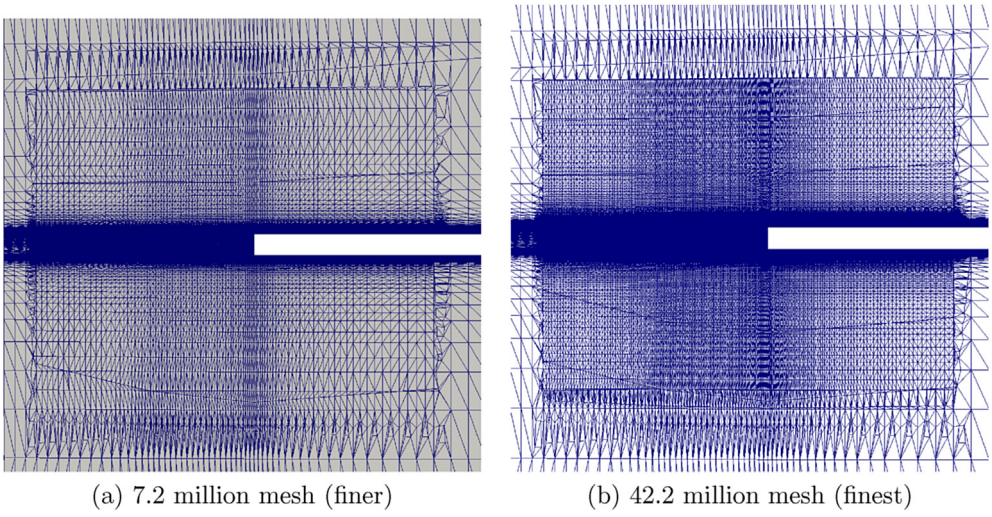

Fig. 4. Meshes with static box refinement at the section $x = c/2$.

node Y^+ is varied between 5 and 40 on the wing for all grids since the refinement is done only in the zone around the tip vortex. Thus, the inner part of the boundary is not resolved and these grids can be ascribed to the so called high *Re* number grids. In this the application of wall functions is necessary. In what follows, for the sake of brevity, the grids are referred to as Hexpress and ICEM grids.

3.2. Improvement of grid resolution using adaptive mesh refinement

Adaptive mesh refinement (AMR) allows one to refine the grid locally within the vortex core using e. g. the Q-criterion. For instance, such a technology developed by Jasak and Tukovic (2010) is based on the computed numerical error gradients in the flow. Each mesh cell was split into two and four subcells in all three directions referring them further as to Q1 and Q2 refinement respectively. This method was applied on the ICEM meshes described above and adapted at each time step. Buffering of the mesh was also introduced which takes into account the refinement layers of the neighbours of the cells which are set for refinement. The mesh gets refined only in the region of the tip vortex as shown (see Fig. 5). AMR was applied only to simulations with curvature corrected turbulence models.

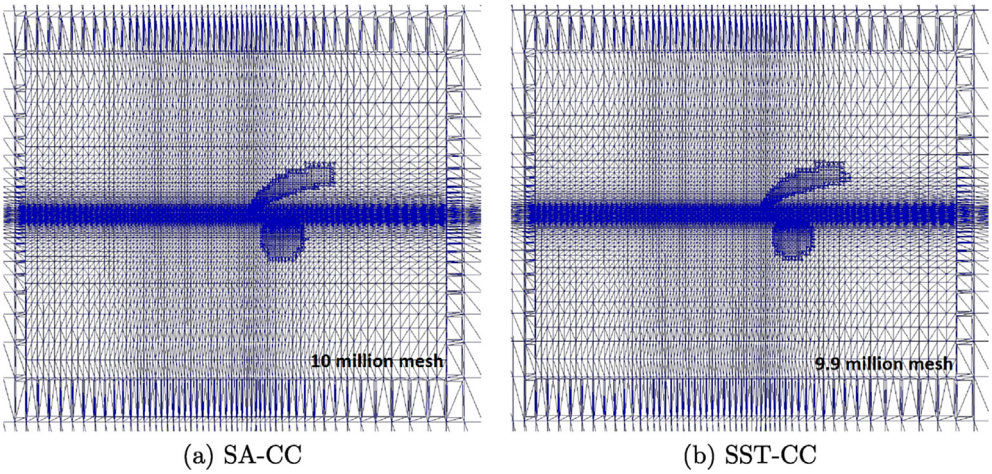

Fig. 5. Grids at x/c = 5 station after application of adaptive mesh refinement.

3.3. Solver settings and turbulence models

Several simulations summarised in Table 1 were carried out. The following paragraphs provide further detailed information on the used numerical methods and models. In case of the unsteady simulations, the flow passed the measurement domain $\Delta x = 30\,c$ (thirty times the chordlength) at least twice and for most cases 3.5 times (for each case, the simulation was stopped when the mean vortex flow converged).

RANS and URANS Models. Several different turbulence models are compared with the same solver settings. The following list gives an overview:

- one-equation turbulence model Spalart Allmaras presented by Spalart and Allmaras (1994) (termed *SA*),
- one-equation turbulence model Spalart Allmaras with curvature correction presented by Shur et al. (2000) (termed *SA-CC*),
- two-equation turbulence model $k-\omega$ -SST presented by Menter et al. (2003a) (termed *SST*),
- two-equation turbulence model $k-\omega$ -SST with curvature correction presented by Smirnov and Menter (2009) (termed *SST-CC*),
- Launder-Reece-Rodi Reynolds stress turbulence model presented by Launder et al. (termed *LRR*).

For the above RANS simulations following settings were taken. The spatial discretisation of the convective term is performed using the filtered Linear scheme implemented in OpenFOAM. This scheme calculates the face values using blending of linear interpolation with a particular amount of upwind, depending on the ratio of the background (in-cell) gradient and face gradient. The amount of upwind is limited to 30%. The laplacian term was discretised using the linear scheme with explicit non-orthogonal correction. Pressure gradient was reconstructed using linear scheme based on the Green- Gauss theorem. The equations for k and ω were discretised in the same manner except the convective term, for which a TVD scheme with Sweby flux limiter was applied.

Without turbulence modelling. As mentioned above, one of a serious disadvantages of turbulence models which leads to a fast vortex decay is the overprediction of the turbulence intensity in the vicinity of the tip vortex core. To analyse this issues, some simulations are carried out without turbulence modelling, i. e. the unsteady Navier-Stokes equations are solved. This can be classified as an underresolved very large eddy simulation (VLES) without a sub-grid model (termed here *w/o*). In case of the 42 M ICEM mesh, the simulation was carried out in an unsteady mode using the PISO algorithm running four times for pressure correction loop to reach convergence. Time derivatives discretisation has been done using the Backward difference scheme and the maximum Courant number was approximately ten. Considering the Hexpress mesh, the time derivatives were discretised like for the hybrid RANS-LES models. See Tab. 1 for an overview of settings.

Table 1
Summary of simulations: meshing tool, wall treatment on the wing, number of cells in millions, turbulence models (w/o: no turbulence model used), time modelling (simulation time/time step in seconds) and Vorticity Confinement method (yes/no).

Mesher	Wall Treatment	# in M	Turbulence Modelling	Time Modelling	VC
Hexpress	Low *Re*	6.0	SA-CC, SST-CC	steady	n
			SA-DDES, SA-IDDES, SST-DDES, SST-IDDES, w/o	Unsteady $(0.6/2.5{\cdot}10^{-4})$	y/ n
ICEM	High *Re*	2.7	SA, SA-CC, SST, SST-CC, w/o	steady	n
		7.2	SA-CC, SST-CC, SA-DDES, w/o, LRR	steady	n
			SA-DDES	Unsteady $(0.6/2.5{\cdot}10^{-4})$	n
		42.2	SA-CC, SST-CC, w/o	steady	n
			w/o	Unsteady $(0.31/10^{-5})$	n

Hybrid RANS-LES Models. Several hybrid turbulence models (termed detached eddy simulation, DES) are used to account for the typical deficiency of standard RANS models which overpredict the turbulence viscosity in the vortex core. This deficiency can be overcome if LES is applied in the vicinity of the tip vortex downstream of the wing. The DES models are based on the one-equation Spalart Allmaras (*SA*, see Spalart and Allmaras (1994)) and the two-equation $k-\omega$ -SST (*SST*, see Menter and Esch (2001)) turbulence models:

- Spalart Allmaras delayed DES presented by Spalart et al. (2006) (termed *SA-DDES*),
- Spalart Allmaras improved delayed DES presented by Shur et al. (2008) (termed SA-IDDES),
- $k-\omega$ -SST delayed DES presented by Gritskevich et al. (2012) (termed *SST-DDES*),
- $k-\omega$ -SST improved delayed DES presented by Gritskevich et al. (2012) (termed *SST-IDDES*).

All simulations with hybrid turbulence models are conducted with the *pimpleFoam* solver, a large time-step transient solver using the PISO and the SIMPLE algorithms, see e.g. Ferziger and Perić (2002). The relaxation factor is set to 0.3 for all variables. During each time step, the SIMPLE algorithm is run 20 times with one pressure correction loop each to reach convergence for the high maximum Courant number of approximately 160. The convection term of the momentum equation is discretised with a linear upwind discretisation scheme (LUDS). The time is discretised using the first order implicit Euler scheme.

3.4. Adaptive vorticity confinement

The approach Vorticity Confinement (VC) describes methods which reinforce vortices and therewith act against the dissipation due to numerical errors. Within all VC methods an artificial source term $\vec{S}$ is introduced into the momentum conservation equations, e. g. for incompressible flow

$$\frac{\partial \vec{u}}{\partial t} + (\vec{u}\cdot\nabla)\vec{u} = -\frac{1}{\rho}\nabla p + \nu\,\Delta\vec{u} + \vec{S}, \tag{1}$$

with the velocity $\vec{u}$, the density ρ, the pressure p and the kinematic viscosity ν. For different VC methods, $\vec{S}$ can be generalised to

$$\vec{S} = \varepsilon\,\vec{s}. \tag{2}$$

The proportionality factor $\in$ (unit m/s) controls the strength of the source term, the vector $\vec{s}$ (unit 1/s) is defined by

$$\vec{s} = \frac{\nabla|\vec{\omega}|}{|\nabla|\vec{\omega}||} \times \vec{\omega}, \tag{3}$$

where $\vec{\omega}$ is the vorticity. Thus $\vec{s}$ points along vorticity magnitude contour lines. (Different formulations of the vector $\vec{s}$ are not considered in this study, because firstly the adaptive VC method - which will be evaluated in this paper - uses the presented formulation and secondly the disadvantages listed subsequently refer to ε and cannot be compensated by another choice of $\vec{s}$.)

The influence of the VC source term was described smartly by Hahn and Iaccarino (2009): Considering an axisymmetric vortex tube, where the vector $\nabla|\vec{\omega}|$ points outward from the vortex centre, the source term convects vorticity back toward the vortex centre as it diffuses outward.

The original VC technique was proposed by Steinhoff and colleagues in 1992 (Steinhoff et al. (1992), Steinhoff and Underhill (1994) and Steinhoff et al. (2005)). The factor $\in$ was set to a user-defined value which is constant over the domain. Several authors improved this

method including the local grid size and vortical fields (like the helicity) in the calculation of the source term. This improves the results of VC, but still there is no universal approach to determine the appropriate value of the user-defined factor. The trial and error approach to find the appropriate value is time-consuming and not reliable. A wrong choice leads to an unphysical vortex flow.

The adaptive VC method introduces a momentum source term counteracting the error of the convection discretisation in an adaptive manner. The magnitude of the source term is proportional to the estimated numerical diffusion defined with the difference between the central scheme (introducing no diffusive error) and the utilised scheme.

Hahn and Iaccarino (2009) proposed the adaptive VC method where $\in$ is determined automatically based on an estimation of the numerical diffusion due to the convective discretisation. This leads to the advantage compared to all other VC methods that there is no need for a user-defined proportionality factor. Furthermore, the target of the adaptive method differs from all others. The adaptive method tries to compensate only for the numerical diffusion due to the convection discretisation whereas all other methods just reinforce vortices to compensate for any kind of dissipation. Accordingly, it might be possible to generate stronger vortices with other methods compared to the adaptive method, but it would be questionable whether the stronger vortex is closer to the physically correct result.

The derivation of the adaptive VC method is based on the estimation of the diffusive truncation error due to the discretisation of the convection term inside the momentum conservation equation with a scheme apart from the central one; Hahn and Iaccarino used the upwind discretisation scheme. This diffusive error $\vec{D}$ is estimated as the difference between two different discretisations of the convection term: the central discretisation (CDS) and the upwind discretisation (UDS) (the latter one should be modified in accordance with the used discretisation scheme within the solver settings)

$$\vec{D} \approx [(\vec{u}\cdot\nabla)\ \vec{u}]^{\mathrm{CDS}} - [(\vec{u}\cdot\nabla)\ \vec{u}]^{\mathrm{UDS}}, \tag{4}$$

which has the unit m/s^2. This approach is consistent with the overall numerical approximation as $\vec{D}$ approaches zero if the corresponding numerical diffusion vanishes (e.g. in case of infinitely fine mesh). The adaptive definition for $\in$ is the dot product of the difference $\vec{D}$ with the vector $\vec{s}$ divided by the squared magnitude of $\vec{s}$.

$$\epsilon = \frac{1}{|\vec{s}|^2}\vec{D}\cdot\vec{s}. \tag{5}$$

For more information on the derivation see Hahn and Iaccarino (2009).

In this study, the adaptive method is used in conjunction with the linear upwind discretisation scheme (termed LUDS). Following, the difference in Eq. (4) is calculated as the difference between CDS and LUDS. Especially if the adaptive method is used in conjunction with high-order convection (HOC) schemes, abrupt local unphysical changes of the sign of $\in$ may occur in the vicinity of the vortex core, see Feder and Abdel-Maksoud (2016a). For that, it is important to modify the adaptive method. An appropriate solution is using the absolute value of $\in$.

$$\vec{S} = |\epsilon|\vec{s}. \tag{6}$$

This still scales with the magnitude of the numerical diffusion and always points along $\vec{s}$, hence convects the vorticity back to the vortex centre and acts against numerical diffusion. Furthermore, the VC source term will be restricted to the vicinity of the vortex. Therefore, the local vortex identification criterion λ_2 will be used (see Jeong and Hussain (1995)): For $\lambda_2 < 0$, the adaptive source term will be set to zero. The influence of the modified source term according to Eq. (6) and due to the restriction of the VC source term have been analysed by Feder and Abdel-Maksoud (2016b).

The following remarks concern the settings of the VC method within the simulations. As the VC source term would introduce huge errors applied in the boundary layer flow, the vicinity of the wing is excluded. The VC source term is faded linearly after a wall distance of $d = 0.01$ m within the layer $0.01\ \mathrm{m} < d < 0.02$ m. Besides, the source term is switched off near the inlet ($x/c < -2$) and outlet ($x/c > 35$) boundaries. Furthermore, in order to smooth the sudden impact due to the activation of the model, the source term is faded in linearly in time within 0.01 s after the simulation without VC has converged.

3.5. Boundary conditions for grid based methods

The boundary conditions (BCs) are defined straightforward with the exception of those for the walls of the wind tunnel: These walls may either be modelled by a no-slip BC to represent the real wind tunnel flow with a closed test section or by a slip BC to save computational effort. The modelling of the boundary layer flow on the wind tunnel walls is expensive because a fine mesh is required: Fig. 6a shows the standard Hexpress mesh presented in Fig. 2 (used with a slip BC on the walls) and subfigure b shows the modified mesh that contains about 4.7 million cells more (corresponding to approximately 80%) to treat the wind tunnel walls. Both meshes are very similar in the vicinity of the wing. The no-slip BC (wind tunnel wall) is modelled via high *Re* wall treatment. In the results section, the influence of the different BCs on the vortex evolution will be analysed (see Section 4.2).

At the inlet the inflow velocity has the fixed value U_∞. The pressure was zero at the outlet and satisfies the zero gradient BC both on the wing and at the inlet. On the wing surface the no-slip boundary condition is enforced. At the outlet the zero gradient BC are enforced for velocity, k and ω fields. Wall functions for k and ω proposed in Menter et al. (2003b) are applied on the wing for the high *Re* number ICEM grids.

3.6. Grid free vortex method

As shown below the application of grid based methods encounter difficulties with the accuracy of vortex tip simulation. Therefore, we have also applied the grid free computational vortex method as an alternative to grid based one. Grid based methods are a very efficient and well developed tool to resolve the turbulent and laminar boundary layers close to the body. On the contrary, the particle based methods have many difficulties with formulation of boundary conditions and smooth representation of thin near wall flows. Therefore there are not much applications of vortex methods for real three dimensional configurations at high Reynolds numbers. However, as will be shown further in this paper, grid based techniques have a substantial artificial numerical viscosity in the wake resulting in a non-realistic damping of vortex structures including tip vortices. A natural way to escape these difficulties and to overcome disadvantages of grid based and particle based techniques is the application of domain decomposition. Close to bodies a grid based method is applied whereas far from the body a grid free one.

In this paper we use the domain decomposition procedure originally developed by Cottet' group (see Cottet and Koumoutsakos (2000), sec. 8.3.2) to improve the resolution of tip vortices by coupling the vortex method and the OpenFoam code. The domain is decomposed into the upstream (zone A) and downstream (zone B) sub-domains (Fig. 7). In the zone A the OpenFoam is used, whereas the flow in the zone B is handled using the vortex method. The outlet conditions for the A-domain solution are taken from the B-domain by direct calculation of velocities induced by vortex elements located in B. The vorticity is calculated at the interface and flows into the domain B where it is handled by a vortex method.

The Schwartz alternating algorithm is applied to match the solutions in A and B at the interface $x = x_1$. The abscissa x_1 is chosen from the condition that the grid based simulation is quite accurate at x_1 and can be used as an initial solution for the grid free method. The vortex elements move and change their strength according to trajectory and vorticity

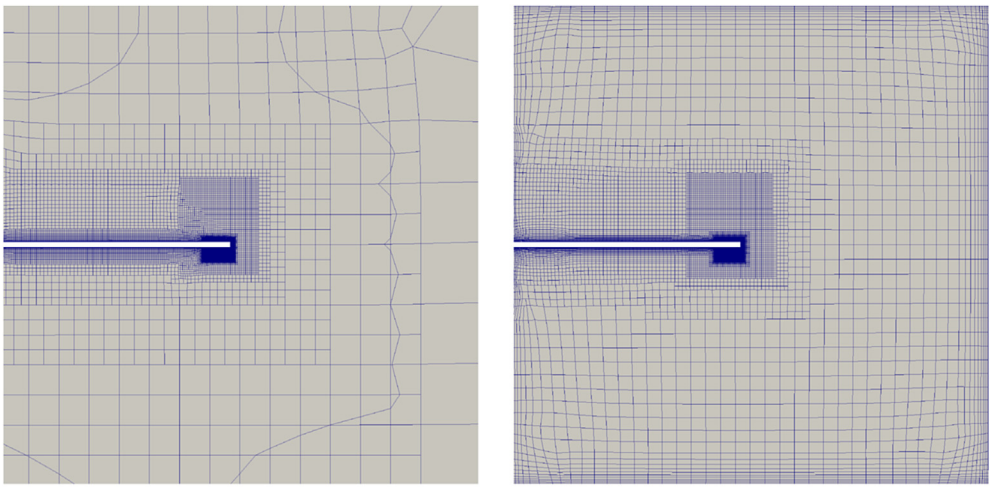

Fig. 6. Hexpress meshes for a different treatment of the wind tunnel walls (view at $x/c = 0.5$).

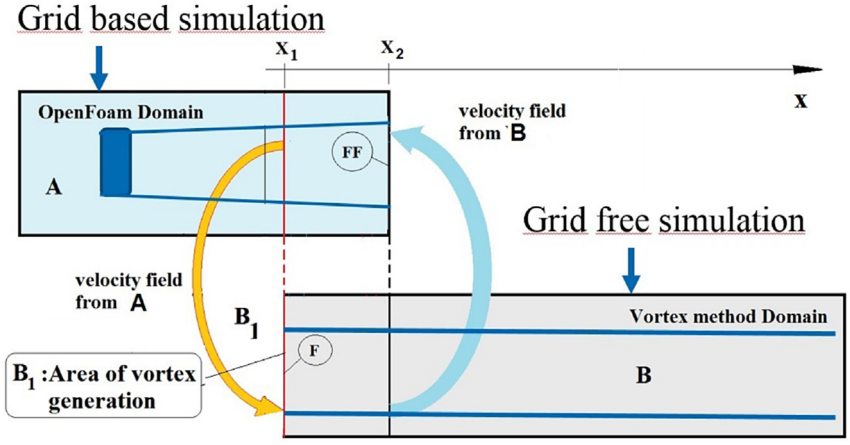

Fig. 7. Illustration of the domain-decomposition method for the tip vortex problem.

transport equations. The particle strength exchange (PSE) method (see, for instance, Cottet and Koumoutsakos (2000)) is applied to take the diffusion effect into account.

The velocity induced by the wing and the tip vortices located in $A' = A - A \cap B$ zone, where $A \cap B$ is the overlapping zone positioned between x_1 and x_2, in the zone B is taken into account by the Poincare identity (see formula (4.3.19) in Cottet and Koumoutsakos (2000)), or by the sources and dipoles continuously distributed on the faces of the A' domain. The source and dipole strengths are equal to the normal and tangential velocities on the faces. The experience shows, that for the problem under consideration an acceptable accuracy is attained if the sources and dipoles are distributed only on the face F, i.e. in the section $x = x_1$. In numerical simulations the continuous distributions are represented by a set of point sources and dipoles located at the centers of grid cell faces within the section $x = x_1$. The distance $x_2 - x_1$ is chosen being equal to the influence length of the source and dipole layers, which is relatively short since the velocity induced by them decays as $\sim r^{-2}$. Like all particle based methods, the vortex element method runs in unsteady mode. The time step is dictated by the accuracy of the calculation of velocities induced at vortex elements by the discrete sources and dipoles. A preliminary study revealed that a proper accuracy is attained at the distance of $\Delta = min(\Delta_y, \Delta_z)$ from the face F, where $\Delta_{y,z}$ are sizes of the cell face. At a smaller distance the velocity rapidly increases due to a singular nature of point sources and dipoles. Larger distances are not desirable because of an overall resolution decrease. From this consideration we get the time step estimation $\Delta t = \Delta / U_\infty$.

The results presented below are obtained using the vortex elements proposed by Winckelmans and Leonard (1993) which induce the velocity at any point $\mathbf{x}_i$ according to formula:

$$\vec{u}_i(\mathbf{x}_i) = \sum_{j=1}^{M} \frac{\boldsymbol{\gamma}_j \times \mathbf{x}_{ij}}{4\pi\sigma_j^3} \frac{\rho + 5/2}{(\rho + 1)^{5/2}}, \tag{7}$$

where $\mathbf{x}_{ij} = \mathbf{x}_i - \mathbf{x}_j$ and $\rho = \left|\vec{x}_{ij}\right|^2 / \sigma_j^2$. σ_j is a size of the vortex element which was taken as $\sigma = \beta\Delta$ where Δ is the size of the grid at the outlet of the A subdomain. The factor $\beta = 2$ secures the overlapping between elements.

Vortex elements are distributed nearly uniformly in space to get a proper element overlapping and stability of simulations (see Cottet and Koumoutsakos (2000)). To fulfill this requirement, the vortices should uniformly be distributed already at the interface B_1. For that the OpenFoam results obtained on a non uniform grid are mapped onto a uniform grid at each Schwartz iteration.

The OpenFoam mapped data are used to generate new vortex elements from the grid based solution using the following procedure. When

the discrete particles are used in the zone B, the most natural condition to set the vortex element strength is

$$\boldsymbol{\gamma}_j = \boldsymbol{\omega}_{OF}(\mathbf{x}_j) Vol_j \tag{8}$$

where $\boldsymbol{\omega}_{OF}(\mathbf{x}_j)$ is the vorticity of the grid simulation at point $\mathbf{x}_j$ and $Vol_j = \Delta^3$ is the volume of cell within which the vorticity is replaced by the $j-th$ vortex element. In what follows the index *OF* stands for quantities of the grid based solution. When the resolution grows $\Delta \to 0$ the vortex elements with the strengths (8) induce the velocity $\mathbf{u}$ which is the same as the grid solution $\mathbf{u}_{OF}$. At moderate Δ for strong concentrated vortices there is a big discrepancy between $\mathbf{u}$ and $\mathbf{u}_{OF}$, namely $\mathbf{u}_{OF} > \mathbf{u}$. To match the velocities at the interface we perform additional adaption at each time instant using the condition of matching between vorticity induced by vortex elements and vorticity of the grid solution

$$\nabla \times \mathbf{u}_{OF} = \nabla \times \mathbf{u} \tag{9}$$

From our experience it is better to use the condition

$$\nabla \times \mathbf{u}_{OF}(\mathbf{x}_i) = \nabla \times P[\mathbf{u}(\mathbf{x}_i)] = \nabla \times P\left[\sum_{j=1}^{M} \frac{\boldsymbol{\gamma}_j \times \mathbf{x}_{ij}}{4\pi\sigma_j^3} \frac{\rho + 5/2}{(\rho+1)^{5/2}}\right], \tag{10}$$

where P stands for the projection of velocities $\mathbf{u}$ onto the grid.

The equations with unknowns $\boldsymbol{\gamma}_j$ (10) can be solved as a system of 3×3 linear equations. However, it is a very consuming procedure. That is why we project (10) on x-axis, since the vector $\boldsymbol{\gamma}$ has a dominant component along x-axis, and use the iteration process:

$$\alpha_i^{(m)} = \alpha_i^{(m-1)} + \varepsilon\left(\nabla \times \mathbf{u}_{OF}(\mathbf{x}_i) - \nabla \times P\left[\sum_{j=1}^{M} \frac{\boldsymbol{\gamma}_j \times \mathbf{x}_{ij}}{4\pi\sigma_j^3} \frac{\rho + 5/2}{(\rho+1)^{5/2}}\right]\right)\mathbf{i}, \tag{11}$$

where ε is relaxation and α is amplification parameter. Once the iteration process is converged, the strengths are updated:

$$\boldsymbol{\gamma}_j = \alpha_j^{(m)} \boldsymbol{\gamma}_j \tag{12}$$

This method, which is very similar to the Beale's iterative method (see Cottet and Koumoutsakos (2000) pages 208–209), has a very good convergence at moderate overlapping β. At large β the accuracy of approximation sufficiently degrades. This is the reflection of the singular matrix problem when the radial based functions with a large overlapping are used for approximation. The vortex method is used without turbulence model, i. e in DNS (direct numerical simulation) mode.

4. Results

4.1. Description of the data evaluation procedure

Numerical results are compared with measurements for the vortex core radius r_1, the peak tangential velocity $V_{\theta 1}$ and the axial velocity at the vortex center U_0. They are extracted from simulations without the correction of vortex wandering, which was not documented in simulations although it occurs under real measurement conditions due to instabilities of the wind tunnel flow and small wing oscillations. The vortex center at each *x*-position is determined by the local minimum of λ_2 criterion in the $x = const.$ plane. The difference in results using any other criterion, for instance *Q* or λ_{ci}, is negligible. The axial velocity U_0 is evaluated at the center. At each radius *r* measured from the vortex center, the tangential velocity is averaged in circumferential direction. The vortex core is defined as the radius r_1 at which the averaged tangential velocity reaches its maximum value.

The vortex core parameters are analysed at the *x*-positions of the measurements $x/c = \{5, 10, \ldots, 30\}$ and additionally at $x/c = \{1.5, 2, 3, 4\}$. Upstream of $x/c = 1.5$ the concentrated tip vortex is hard to identify since the roll up process is not completed. If the core radius exceeds $0.4\,c$ at large distances from the wing, the vortex core parameters are not evaluated, because the vortex becomes too smooth and dissipates to a weak level. The evaluation of the unsteady simulations starts after 0.6 s. In this time, the flow passes the distance of interest $x/c = 30$ more than three times what is enough to exclude the start-up transitional phase.

The unsteady simulations results are averaged in time within the period of 0.1 s, which is large enough to guarantee the convergence of statistical data.

For a proper validation, it is important to compare our results not only with measurements but also with other numerical simulations. Unfortunately, we found only one available simulation data for the Devenport et al. test case performed by Wells et al. (2010), who applied various turbulence models to assess their performance in predicting a tip vortex flow: the one-equation model of Spalart Allmaras (with and without curvature correction) and the Reynolds stress transport model (RSM) LRR proposed by Launder et al. (1975). A structured mesh with 11.9 M cells and wall functions for the resolution of the boundary layer flow on the wing were utilised. Unfortunately, there is no information available on the grid resolution in the vicinity of the vortex core. Wells determined the tip vortex parameters in a slightly different way than in this study. The vortex center is determined by the maximum helicity. The tangential velocity profile used to determine r_1 and $V_{\theta 1}$ is evaluated only along one line parallel to the *z*-axis through the vortex core without averaging in circumferential direction. The main conclusion of his work is the superiority of the RSM model in comparison with others. Its application leads to results which match very well the experimental ones at small x/c. Unfortunately, no information is presented downstream of $x/c = 10$, because of strong dissipation of the tip vortex in the far field.

4.2. Influence of the boundary condition of the wind tunnel walls

This section deals with the influence of different boundary conditions (BCs) applied to the wind tunnel walls: slip or no-slip ones. Devenport et al. (1996) observed a slight streamwise pressure gradient ($dC_p/dx = -0.3\%\ m^{-1}$) along the wind tunnel due to the evolution of the boundary layer. This obvious phenomenon leads to an acceleration of the flow. The question is whether the boundary layer evolution on the tunnel walls needs to be considered for a proper prediction of the tip vortex evolution.

Therefore, two simulations will be carried out on the no-slip mesh (see Fig. 6b) using the SA-DDES turbulence model: one with a slip and one with a no-slip BC realised on the tunnel walls. Following the high-Re wall treatment of the tunnel walls, the mean (max) Y^+ -value is about 95 (150) and justifies the use of wall functions for the attached boundary layer flow. The numerical settings are similar to the ones used for the hybrid RANS-LES turbulence models on the Hexpress slip mesh.

The influence of the different boundary conditions on the vortex strength (until $x/c = 30$) is negligible: Comparing with the no-slip condition, the core radius increases by about 0.2% and the peak tangential velocity decreases by about 0.8% for the slip condition. Both values show no clear tendency behind the wing. Besides, the axial velocity (at the vortex centre) decreases by about 1.4% using the slip condition, the difference between the slip and no-slip result increases monotonously in the streamwise direction. Both points are reasonable because the boundary layer evolution accelerates the free flow.

Thus, the neglected boundary layer evolution leads to a slight deceleration of the axial vortex flow and can be considered in simulations. However, the slip BC is proven to be sufficiently accurate for the objective of the current paper: comparison of different approaches to predict a tip vortex flow. Hence, it will be used in the following simulations.

4.3. Comparison of different turbulence models on ICEM and Hexpress meshes

4.3.1. ICEM mesh

Fig. 8 illustrates the influence of the mesh resolution and the curvature correction for the ICEM mesh. First of all, it is to note a strong degradation of the concentrated tip vortex in the far wake field. The maximum tangential velocity, and, consequently, the vortex strength, losses about two thirds of its initial value whereas the vortex core is spread up with the factor of four and more. Large discrepancy between measurement and simulations underlines the importance of the problem considered in the present paper. Simulations are not capable of predicting the tip vortex flows at distances from the wing $x/c > 5$ which are relatively moderate and quite typical for marine applications. For instance, helicoidal tip vortices of propellers interact with rudders in the far vortex wake. Therefore, such a discrepancy makes impossible numerical analysis of some important practical problems, for instance, of the tip vortex cavitation influence on the rudder erosion. In this paper, we are going to clear which models and grids are able to improve the simulation accuracy. Grid independence study showed that convergence is attained on the grid with 7.2 million cells with and without curvature correction models. For this resolution the influence of the curvature corrections is positive but insufficient for a radical improvement of the modelling accuracy. As seen, the confining effect of both curvature correction models on the vortex radius is big at coarse resolution (2.7 M) and becomes negligible at finer resolutions. It is hard to find any

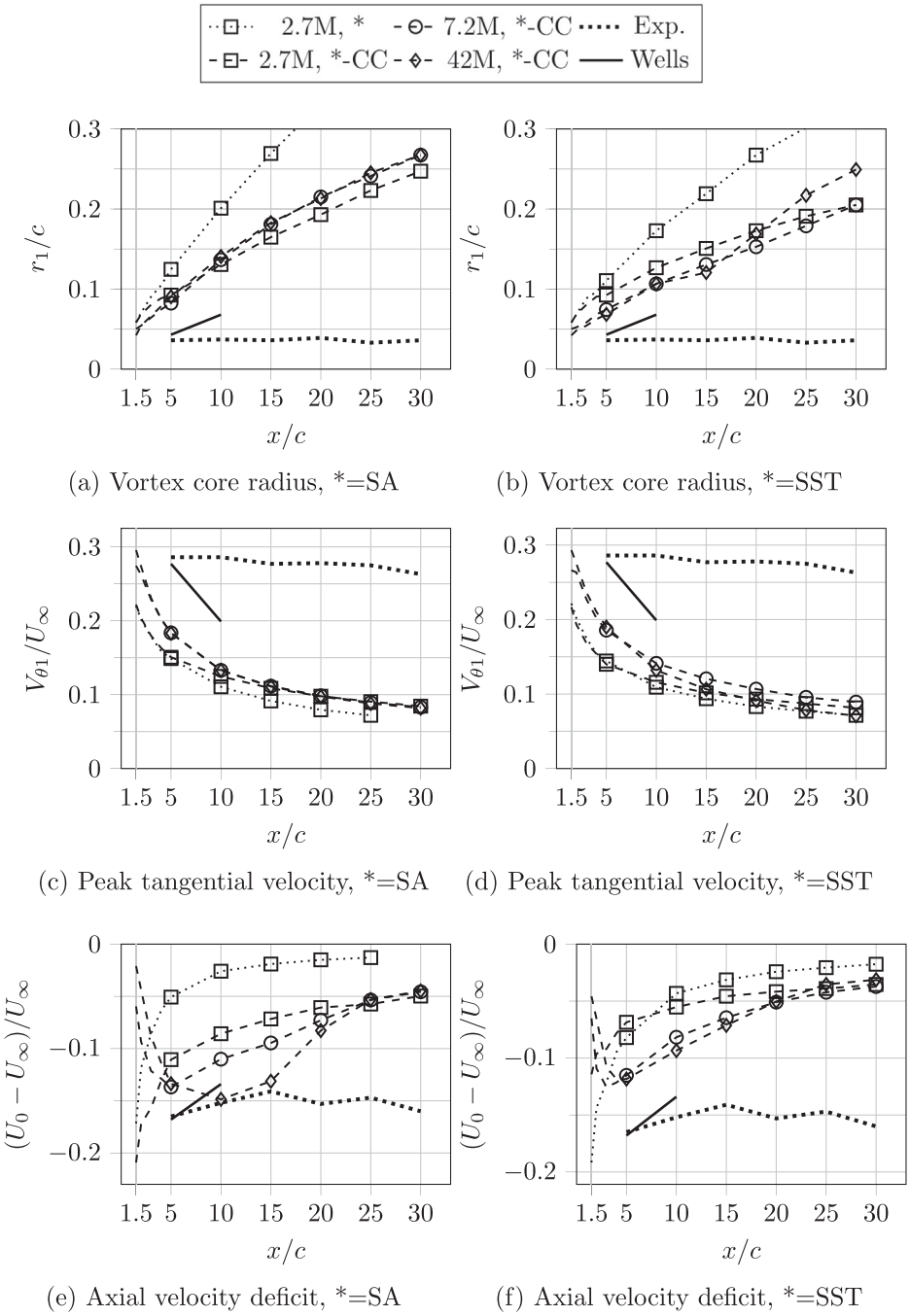

Fig. 8. Influence of mesh refinement and curvature correction on vortex core parameters for different turbulence models based on Spalart Allmaras (SA) and $k-\omega$ -SST (SST) (considering the ICEM meshes).

advantage of one model with respect to the other. Their effects are comparable.

Fig. 9 shows the comparison for the core parameters obtained using different turbulence models. Among these turbulence models LRR yields the best result. The reason is that the RSM models take the anisotropy of the flow into account and the consideration of the rotation effects is an inherent part of the modelling. Unfortunately, the application of the RSM has a strong limitation because of numerical instabilities which were documented in our case at meshes finer than 7.2 million cells. The most promising results were obtained using no turbulence model (termed *w/o*). As seen in Fig. 9, the lowest rate of vortex decay occurs without turbulence modelling followed first by LRR and then by SA-DDES. Fig. 8 shows that the turbulence models based on one- and two-equation eddy viscosity models with curvature correction lead to inferior results. The strong decay of the vortex strength and the vortex core spreading downstream of $x/c = 20$ illustrated in Fig. 9), is due to coarsening of the grid at $x/c > 20$. Here it should be noted that, as stated by Devenport et al. (1996), the flow on the wing and the tip vortex depend on the tripping of the boundary layer on wing. At $x/c = 10$, for different locations of tripping the radius r_1 is changed between 0.033 and 0.037, whereas without tripping it was 0.038. The tangential velocity is varied between 0.263 and 0.286 being equal to 0.291 without tripping. These differences are around ten percent and cannot be used as an explanation of big discrepancy between numerical results with and without turbulence modeling. The parameter most affected by the turbulence tripping is the axial velocity since its distribution is strongly dependent of the wing boundary layer which is in turn depends on the flow regime on the wing. With tripping the axial velocity deficit $(U_0 - U_\infty)/U_\infty$ is varied between -0.152 and -0.182 whereas it is two times less without tripping -0.086. The latter value is in a good agreement with the solution obtained on the

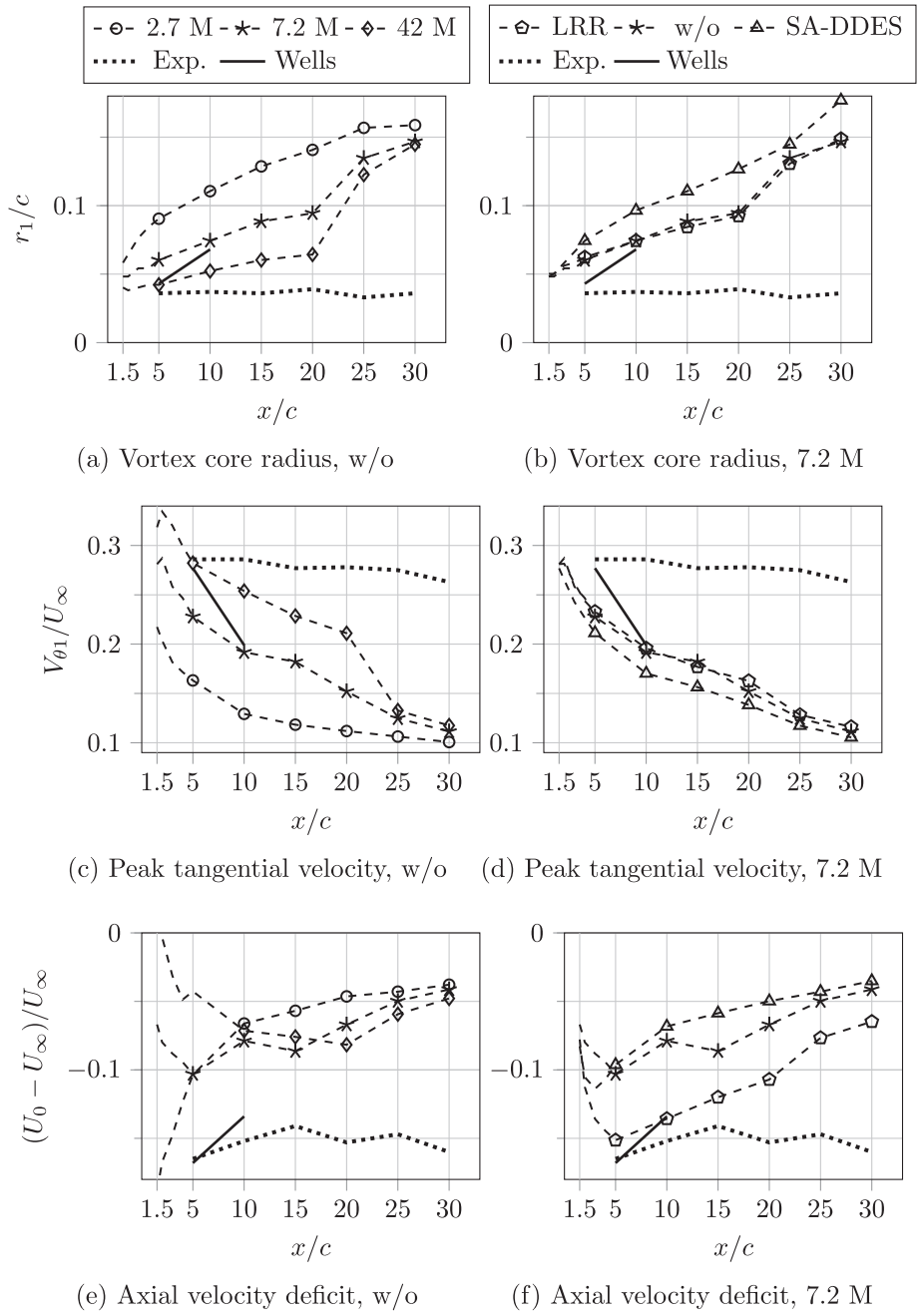

(a) Vortex core radius, w/o (b) Vortex core radius, 7.2 M

(c) Peak tangential velocity, w/o (d) Peak tangential velocity, 7.2 M

(e) Axial velocity deficit, w/o (f) Axial velocity deficit, 7.2 M

Fig. 9. Influence of different turbulence models on the vortex core parameters. The left figures present the results obtained without turbulence modelling on different ICEM meshes, whereas the right figures show the results obtained on the ICEM mesh with 7.2 M cells and different turbulence models (including the approach without turbulence modelling (*w/o*)).

finest mesh without turbulence modelling (Fig. 9).

The circulation Γ was found using the classical definition $\Gamma_R = \oint V_\theta \, dC_r$, where C_r is the circle with the radius r/c. Numerical integration along the circle is performed using $L = 360$ points. The velocity V_θ at the points is calculated using a linear interpolation between neighbouring grid cell centres. Increase of L doesn't lead to the increase of accuracy because the distance between the integration points is smaller than grid cell size. The circulation of the solution without turbulence modelling inside of the tip vortex is higher than this of the solutions based on turbulence models what is in accordance with relations stated above for the tangential velocity. Outside of the vortex core at $r/c > 0.05$ the circulation Γ obtained without a turbulence modelling approach is proved to be smaller than these of the turbulent calculations. It can be explained as follows. As seen in Fig. 10, the roll up process is not completed up to $x/c = 5$ and the circulation continues to grow in the range up to $r/c = 0.5$ due to vortex sheet shed from the trailing edge. Contrary to the turbulent solution, the solution without turbulence modelling is very unsteady with creation of vorticity of opposite signs in the vortex sheet. The contribution of the sheet vorticity with rotations opposite to this of the tip vortex reduces the growth of the circulation and makes its dependency on r non monotonic. As result, Γ of the 'w/o' model solution becomes smaller outside the vortex core.

Increase of resolution in turbulent simulations from 7.2 M to 42 M of cells, which reduces the discretisation errors and artificial viscosity, show no improvement in the numerical results. Therefore, the superiority of the solution without turbulence modelling leads to the conclusion that this model is physically more relevant than turbulent models and the flow inside the tip vortex is rather laminar than turbulent although the Reynolds number is high enough to expect the turbulent character of the flow both on the wing and in the wake. This simulation supports the conclusion of Devenport et al. (1996) that "flow in the core is laminar and that velocity fluctuations experienced here are inactive motions produced as the core is buffeted by turbulence from the surrounding wake". The shapes of the profiles do change, however, and at a rate that is not inconsistent with laminar diffusion (Devenport et al. (1996)).

4.3.2. Hexpress mesh

Fig. 11 shows the influence of different turbulence models on the evolution of the tip vortex core parameters: both Spalart Allmaras and $k-\omega$ -SST with curvature correction (CC) and hybrid models with improved delayed DES (IDDES) as well as delayed DES (DDES) models, besides the approach without turbulence modelling (termed *w/o*) is considered too. A peculiar point about these results is that SA-CC leads to an overprediction of the axial velocity deficit. Considering both other vortex core parameters shows that the agreement with the experimental

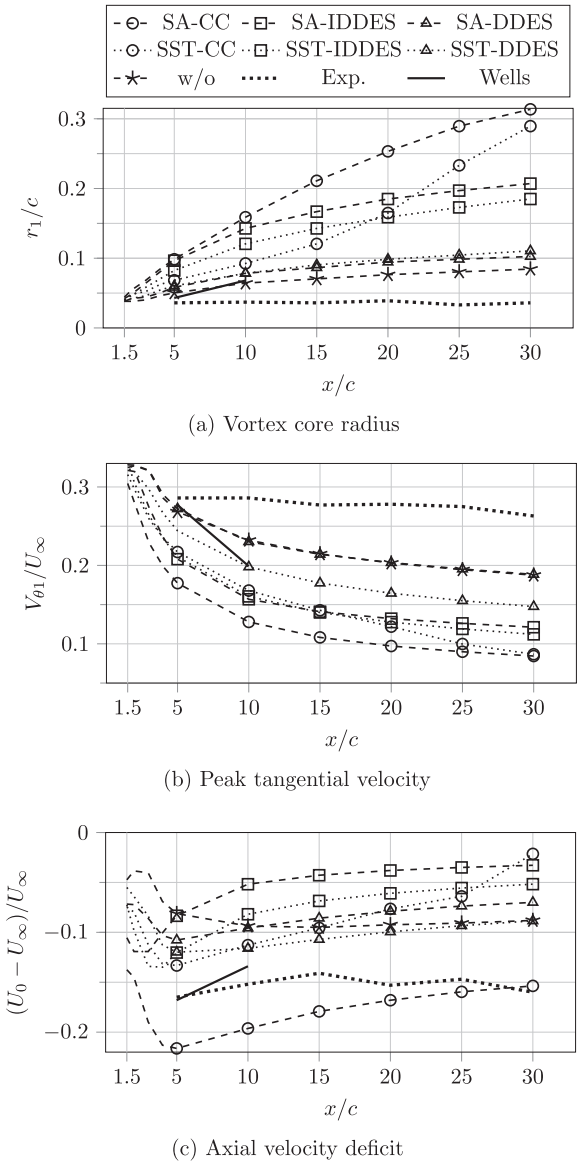

(a) Vortex core radius

(b) Peak tangential velocity

(c) Axial velocity deficit

Fig. 11. Influence of different turbulence models on the vortex core parameters. The results are obtained with the Hexpress mesh.

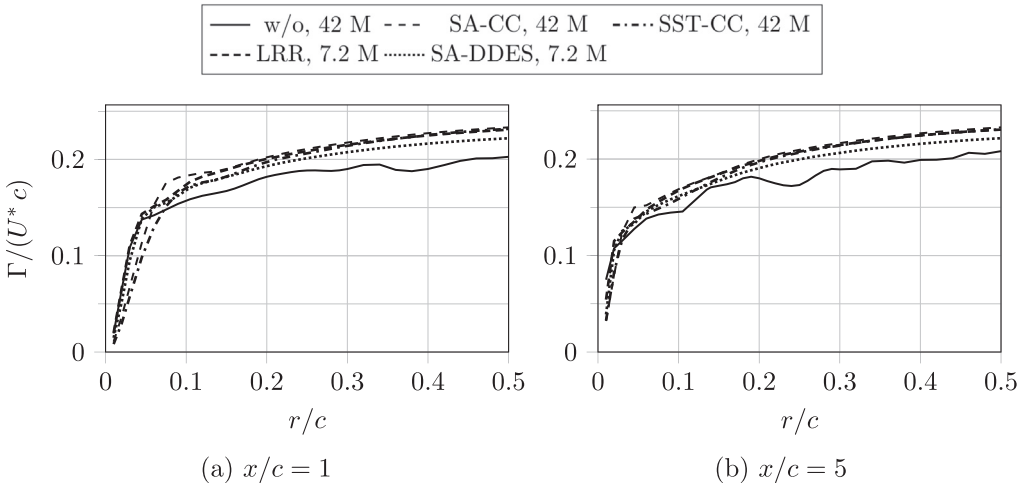

(a) $x/c = 1$ (b) $x/c = 5$

Fig. 10. Figures showing circulations of the tip vortex with the radius chord distance at $x/c = 1$ and $x/c = 5$.

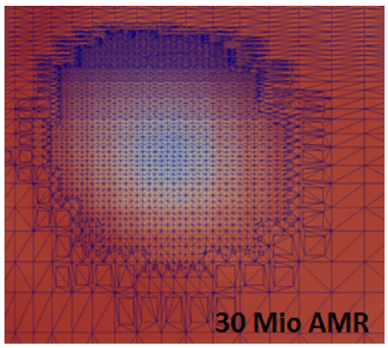

Fig. 12. Mesh distribution using AMR in the vicinity of the vortex core.

results is worst for SA-CC model. A possible reason is the overestimation of the boundary layer thickness in the Spalart Allmaras model resulting in overestimation of the vortex radius and axial velocity deficit. The use of $k-\omega$ -SST leads to a stronger vortex compared to the result gained with Spalart Allmaras in case of SST-CC and SST-IDDES, but not in case of SST-DDES: SA-DDES is more accurate. The strongest vortex (and therewith the highest accuracy concerning the core size and the peak tangential velocity) is obtained without turbulence modelling: compared to SA-DDES the core is smaller and the peak tangential velocity is equal. Comparing the result obtained without turbulence modelling with the experimental one at $x/c = 30$, the core radius is about 2.3 times larger, the peak tangential velocity is about 29% smaller and the axial velocity is about 8.6% higher (the axial velocity deficit is about 45% smaller) for the numerical prediction. Although the deviation of the nondimensional axial velocity deficit between the numerical predictions and the experimental value is quite high (around 50% and more), the deviation of the predicted axial velocity itself is much lower (deviation around 10%). Considering the mesh refinements of the ICEM mesh or that of the Hexpress mesh in Feder and Abdel-Maksoud (2016b), the accuracy of the core radius and peak tangential velocity prediction can be significantly increased refining the mesh in the vicinity of the tip vortex (for the DES models and the approach without turbulence modelling).

Wells (2009) evaluates the simulation results only until $x/c = 10$, as he remarks excessive dissipation of the tip vortex further downstream. This can be seen in Fig. 11. Especially the decrease of the peak tangential velocity is very high compared to the results obtained within this study. Nevertheless, the accuracy of all three vortex core parameters at $x/c = 5$ is very good and the result is clearly superior in comparison to the results obtained here. A possible explanation for the decrease between $x/c = 5$ and $x/c = 10$ is a change in the mesh (coarsening). Unfortunately, Wells (2009) provides no detailed information concerning the mesh density in the vicinity of the vortex core which would allow to draw more detailed explanations of the difference between both simulations.

4.4. Potential of adaptive mesh refinement

Fig. 12 shows the ICEM mesh after the adaptive refinement in the vicinity of the vortex core resulting in the mesh with 30 million of cells. The initial mesh before refinement contains 7.2 M of cells. The mesh topology at the boundary of vortex is skewed which could cause numerical errors negatively affecting the solution accuracy in the area surrounding the vortex core. Unfortunately, the hope to improve the accuracy of the simulation using AMR in the vortex core was not justified. As seen in Fig. 13 the application of the AMR has a negligible positive effect on the calculation results.

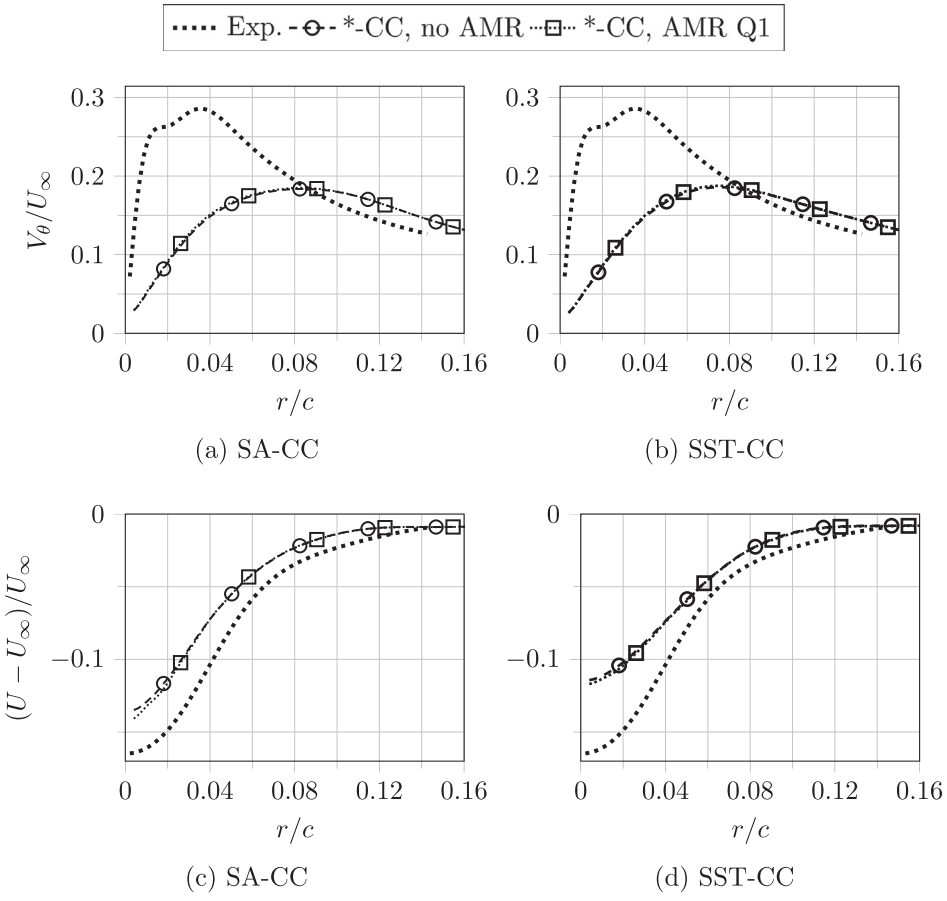

Fig. 13. Influence of AMR on the tangential and axial velocity profiles through the vortex core at $x/c = 5$.

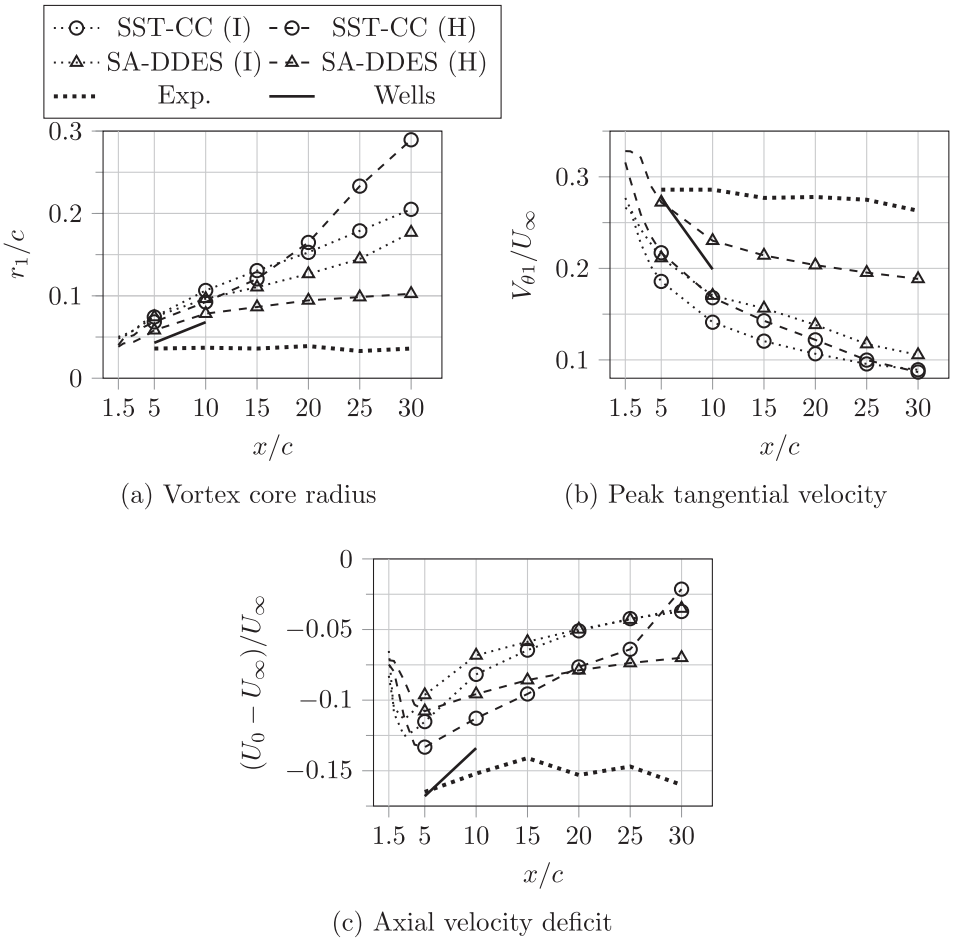

(a) Vortex core radius (b) Peak tangential velocity

(c) Axial velocity deficit

Fig. 14. Influence of different mesh types on the vortex core parameters, I: ICEM with 7.2 M, H: Hexpress with 6.0 M mesh cells.

4.5. Comparison of results for two meshes: 7.2 M (ICEM) and 6.0 M (Hexpress)

The tangential velocity close to the wing is proportional to the vortex circulation and, therefore, to the lift. The lift coefficient of the wing using the VLES (w/o, without turbulence modelling) approach on the fine ICEM mesh (42 million grid points) is around 0.46. This value is equal to this obtained from the panel code Autowing, see Kornev (2016). For the cases run on the ICEM meshes based on two-equation turbulence models (and the DES version) the lift coefficient is between approximately 0.41 and 0.42 (larger lift for the finer meshes). The turbulent simulations on the Hexpress grid provide a lift coefficient between approximately 0.45 (turbulence models based on SA and VLES) and 0.47 (based on SST) which is roughly ten percent higher compared to the ICEM meshes and similar to C_L from the panel method. We suppose that at small angle of attack of 5° the lift coefficient should be independent on the viscous effects. Therefore the results for inviscid flow and flow with and without turbulence modelling should be close to each other. A possible reason for the low lift coefficient on the ICEM grid is the inaccuracy in the turbulent boundary layer modelling using wall functions applied in the buffer zone region between $5 < Y^+ < 30$. As a result, the boundary layer thickness is overestimated what results in the overestimation of the displacement effects and reduction of the lift coefficient.

While on the ICEM grid both models SA-CC and $k-\omega$ -SST-CC provide almost the same results at moderate and fine resolutions, there is a big difference between two models on the Hexpress grid (see Fig. 11). This can be explained by different treatment of the boundary layer on the wing. On ICEM grid the inner part of the layer is modelled by wall function making the difference between models negligible. When the boundary layer is well resolved the advantage of the $k-\omega$ -SST approach for boundary layer modelling comes into play. The thickness of the boundary layer, which has a strong impact on the tip vortex core radius, is predicted more accurately by the $k-\omega$ -SST model. The core radius from SA model is obviously overestimated with respect to both measurement and $k-\omega$ -SST results what leads to the underestimation of the tangential velocity. As result, the accuracy of the $k-\omega$ -SST-CC model outperforms this of the SA-CC model. With the other words, the advantages of the $k-\omega$ -SST-CC model are due to advantages of the pure $k-\omega$ -SST model over the pure SA model.

Fig. 14 shows the influence of different meshes for two turbulence models: $k-\omega$ -SST with curvature correction and Spalart Allmaras delayed DES. For the Hexpress mesh, the length of the mesh cells l in the vicinity of the tip vortex core (in the x-plane) is about $l/c = 0.0088$. For the ICEM mesh with 7.2 M cells, the cell size changes in the vicinity of the vortex (in the x-plane), because of the mesh structure. The average cell size is approximately $l/c = 0.01074$, i.e. about 22% larger than for the Hexpress mesh.

Based on the results gained with the DES approach, it is clear that the result on the Hexpress mesh is superior compared to the one on the ICEM mesh. The core size is smaller, the peak tangential velocity is higher and the axial velocity deficit is also smaller. All this results in a smaller discrepancy with experimental data for each quantity. One reason for the superiority of the Hexpress mesh might be the increased mesh density in the vicinity of the vortex core. Another possible reason is the different wall treatment. ICEM mesh has large Y^+ values and requires utilisation of wall functions whereas fine resolution of the turbulence boundary layer

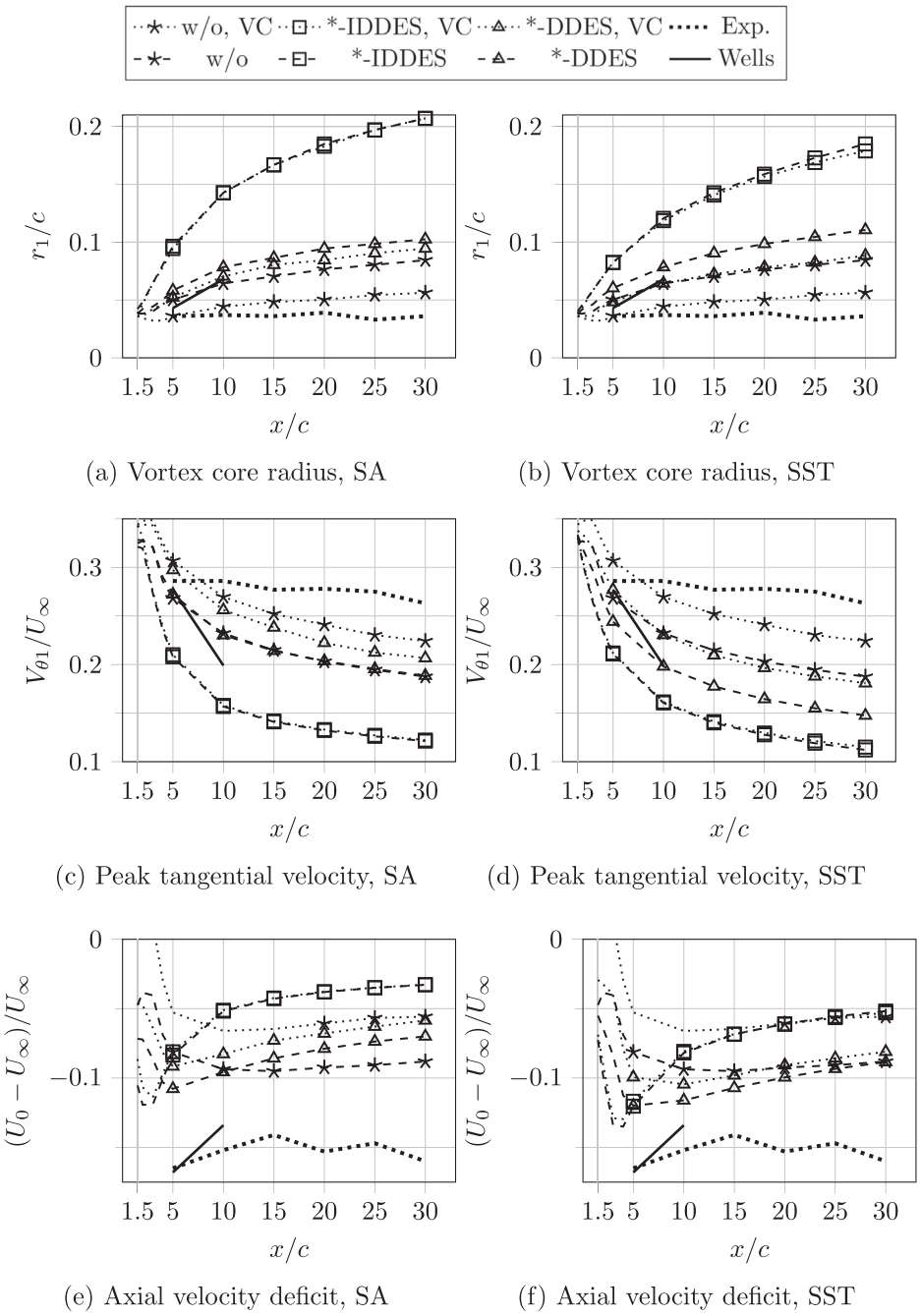

Fig. 15. Influence of VC on the vortex core parameters for different DES-models based on Spalart Allmaras (SA) and $k-\omega$ -SST (SST) (Hexpress mesh with low *Re* wall treatment).

is performed on Hexpress mesh.

4.6. Potential of vorticity confinement

Feder and Abdel-Maksoud showed in Feder and Abdel-Maksoud (2016a) for the Devenport test case that the potential of VC depends on the turbulence modelling. For the standard Spalart Allmaras model the increase of the vortex strength was much less compared to the increase using Spalart Allmaras delayed DES. A possible reason for the strong dissipation of the tip vortex is the huge overprediction of turbulence intensity created by the Spalart Allmaras model. This also leads to a small VC source term which is proportional to the vorticity. Hence, the numerical diffusion due to the overprediction of the turbulent viscosity cannot be balanced by VC.

In this section, the potential of the adaptive VC method in conjunction with SA/SST-IDDES and SA/SST-DDES and an approach without turbulence modelling (termed *w/o*) is compared. The vortex core parameters are shown in Fig. 15. Firstly, the influence of VC on the vortex is negligible in case of SA/SST-IDDES compared to the effect in case of SA/SST-DDES. A possible explanation is that the vortex is considerably weaker in case of SA/SST-IDDES without VC (about twice the core radius and about two third to three quarter the peak tangential velocity of the result of SA/SST-DDES). Hence, as the VC source magnitude is proportional to the vorticity, the source term is smaller and therewith the effect of VC.

Considering the approaches based on DDES and without turbulence modelling, the application of VC leads to a significant reduction of the vortex core radius and a significant increase of the peak tangential velocity. Besides, the axial velocity (at the vortex centre) is increased also. In the following, the effect of the VC method will be described in detail using the relative change of the core parameters (r_1 and $V_{\theta 1}$) at the

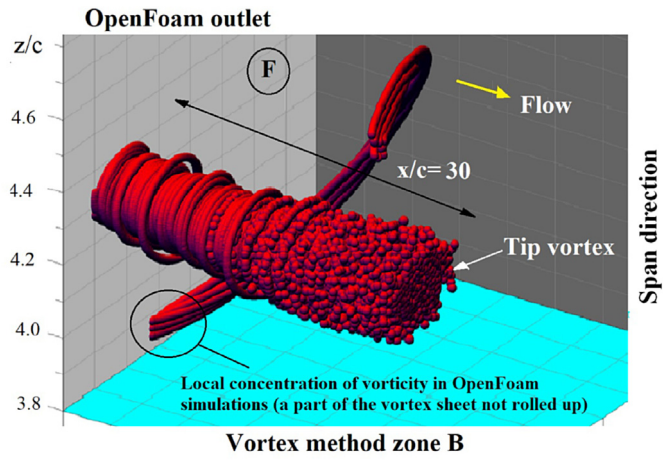

Fig. 16. Instantaneous distribution of vortex elements in grid free Lagrangian simulation. The radius of bubbles is proportional to the vortex element strength.

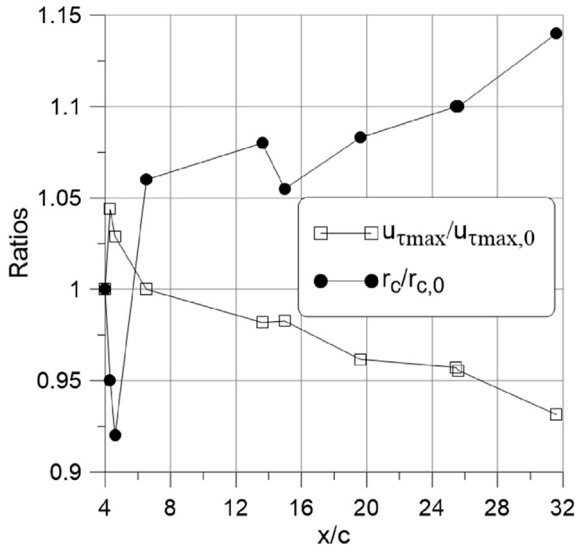

Fig. 17. Results of pure Lagrangian simulations. r_c is the radius of the tip vortex, $u_{\tau max}$ is the maximum tangential velocity. The lower index 0 stands for the value at the inlet of the vortex method computational domain.

measurement points $x/c = \{5, 10, \ldots, 30\}$. For both IDDES turbulence models, the effect is negligible (less than 2%). For the approaches SA-DDES, SST-DDES and without turbulence modelling the core radius is reduced in average by about 9%, 20% and 32% respectively. The peak tangential velocity for these approaches is increased in average by about 10%, 19% and 17%.

The results of SA-DDES and SST-DDES with VC are comparable (considering the core size, one turbulence model is superior, considering the peak tangential velocity, the other one is superior). However, the SST-DDES model shows higher accuracy in terms of the axial velocity which leads to its overall superiority.

The strongest vortex (in terms of small core size and high rotational velocity) is obtained without turbulence modelling (VLES approach) and VC which leads also to the smallest error compared to the experimental results.

Feder and Abdel-Maksoud (2016b) analyse the potential of the adaptive VC method in conjunction with different resolutions of the mesh in the vicinity of the tip vortex. Therefore, the SA-DDES turbulence model with the same settings for the same test case is used. The results show that the relative change of the core radius and the peak tangential velocity due to the application of the adaptive VC method is nearly equal if the cells in the wake are refined or coarsened by the factor two.

4.7. Grid free Lagrangian simulations using computational vortex method (CVM)

The previous results gained with grid based methods showed that the vortex decay is large in each case compared to the experimental result. The reason for that is the inherent numerical diffusion due to insufficient mesh resolution and insufficiently accurate turbulence modelling. Therefore, the potential of grid free vortex methods will be evaluated in this section. The algorithm presented in Section 3.6 was implemented into OpenFoam toolkit.

Results obtained using Lagrangian simulation are presented in Figs. 16 and 17. The grid used was uniform with the size $\Delta_{x,y,z} = \Delta$. Velocity field necessary for inlet conditions at the interface between OpenFoam and CVM domain was mapped onto the uniform grid. The ordinary differential equations describing the particle motion are integrated using the predictor-corrector or Euler corrected method with the trapezoidal rule. As mentioned above, the time step Δt is chosen so that the particles paths close to the interface within Δt is around Δ, i.e. $\Delta t = min(\Delta/(U_\infty + u_x))$, where u_x is the perturbation velocity induced by vortex and wing. In simulations, presented below, it was around $\Delta t = 1.04 \cdot 10^{-4} s$. To reduce the computational time the number of vortex element is limited. When the vortices are identified at the interface F from the OpenFoam solution, only vortices with the vorticity magnitude larger than 10 percent of the maximum vorticity enter into the domain B.

The discrete vortices at the interface F at $x/c = 4$ are determined on the uniform grid with the size Δ using the matching algorithm described above. The grid free simulation was matched with the OpenFoam grid simulation using $k - \omega$ SST model with 7.2 M cells. At $\Delta/c = 2E - 2$ the computational domain of the vortex method is occupied by 86,500 vortex elements with 61 elements in the tip vortex cross section at $x/c = 4$ (see Fig. 16). The vortex core parameters presented in Fig. 17 were obtained by averaging within 0.01 s.

The maximum tangential velocity related to that at the interface between the grid based and grid free computational domains is presented. A similar ratio is presented for the vortex core radius. It should be noted, that, despite a discrete representation of vorticity by vortex elements, the distribution of the velocity and radius remain smooth and regular up to the end of the computational domain excepting a very short initial range close to the interface. The reason is the transition of the solution from the grid based to the grid free ones which is still not accurately simulated due to discrete representation of the continuous source and dipole layers and an inaccuracy in matching between two computational domains.

As seen from Fig. 17 the radius of the tip vortex is slightly grows by fourteen percent along the whole computational domain at $4 < x/c < 34$. The maximum tangential velocity decreases only by seven percent at the end of the domain. This is the best numerical solution obtained so far. It shows a strong potential of the grid free method to radically improve the quality of numerical simulation of the tip vortex flow. However, this method has two substantial restrictions. First, since the method has a sufficiently reduced numerical viscosity, the stability of the pure Lagrangian simulation can be critical for strong concentrated vortices at large Reynolds numbers. Second, improvement of the tip vortex resolution by increase of particle number is limited due to high computational costs when the particle number increasing. Therefore, study of the CVM method properties as well as the development of efficient algorithms will be continued in the future works of the authors.

5. Conclusions

A proper prediction of the tip vortex evolution is a big challenge for computational fluid mechanics despite of many efforts to solve this classical problem having a big practical importance in aerodynamics and

hydrodynamics. In numerical simulations the tip vortex rapidly degrades loosing its strength and spreads up already at distances of a few dozens of the wing chord. As a result, numerical analysis of important practical problems, for instance, of the tip vortex cavitation influence on the rudder erosion with an acceptable accuracy becomes impossible. In this paper, we tried to find an efficient way to improve the simulation accuracy using different numerical methods, grids and turbulence models.

It was shown that the application of curvature correction (CC) to standard two-equation turbulence models of Spalart Allmaras and $k-\omega$ SST improved results at a rate which depends on the grid. For the coarse grid the improvement is substantial. For fine grids with large Y^+ and an approximate treatment of the boundary layers using wall functions the influence of the curvature correction is negligible. On the contrary, the grids with well resolved boundary layer and small Y^+ show a strong sensitivity to curvature corrections. The $k-\omega$ SST model with curvature correction (according to Smirnov and Menter (2009)) has a clear advantage over the corrected Spalart Allmaras model. In conjunction with adaptive mesh refinement (AMR) these turbulence models showed insignificant improvement for fine grid resolution. The performance of the detached eddy simulation models like DDES and IDDES is proved to be much better than this of the one and two-equation turbulence models. The highest accuracy among DES models is provided by the delayed DES approach which prevents the vortex from large diffusion. The highest accuracy among all (U)RANS turbulence models is attained with the LRR Reynolds stress transport models (RSM) which takes the anisotropy of the turbulent wake into account and the rotation effects are an inherent part of modelling in this technique. The most promising results among grid based methods were obtained using the approach without turbulence modelling, which can be classified as an underresolved very large eddy simulation without a subgrid model.

The superiority of this solution leads to the conclusion that the used turbulence models do not reproduce the flow relaminarization in the vicinity of the tip vortex core which is the reason for the very slow tip vortex decay. This simulation supports the conclusion of Devenport et al. (1996) that the "flow in the core is laminar and that velocity fluctuations experienced here are inactive motions produced as the core is buffeted by turbulence from the surrounding wake". This fact explains also the improvement of numerical solution when DES is applied. Indeed, in DES the turbulent viscosity within the tip vortex is reduced by switching the turbulent solution to LES one. In this way, the total viscosity approaches to the laminar one and the accuracy of the numerical solution is improved.

The potential of the adaptive vorticity confinement method depends on the underlying turbulence model. Its application reinforced the vortex flow but also can lead to an acceleration of the axial flow component. A further extensive investigation is needed to determine the drive mechanism for this acceleration.

To further reduce the artificial vortex diffusion, a pure Lagrangian grid free vortex method is applied to simulate the tip vortex dynamics in the far wake. Grid free simulation is coupled with the grid based one in the near wake, where the vortex diffusion can be considered as small. The flow on the wing and in the near wake is treated using grid based method, whereas the remaining flow part is calculated using the grid free approach. Grid free vortex method provides the most promising results showing the lowest rate of the vortex strength decay and vortex core spreading. However, this method has two substantial restrictions. Firstly, since the method has a sufficiently reduced numerical viscosity, the stability of the pure Lagrangian simulation can be critical for strong concentrated vortices at large Reynolds numbers. Second, improvement of the tip vortex resolution by increase of particle number is limited due to high computational costs when the particle number increasing. Further development of the grid free vortex and grid based vortex confinement methods as well as their coupling seem to be a very promising way for a radical improvement of the accuracy of tip vortex dynamics prediction.

Acknowledgments

The support of the authors by the German Research Foundation (Deutsche Forschungsgemeinschaft) under the grants AB 112/10-1 and INST 264/113-1 FUGG is gratefully acknowledged.

References

Birch, D., Lee, T., 2005. Tip vortex behind a wing oscillated with small amplitude. J. Aircr. 42 (5), 1200–1208.
Chow, J.S., Zilliac, G., Bradshaw, P., 1994. Turbulence Measurements in the Near-field of a Wingtip Vortex, vol. 203. ASME-Publications-FED, 61–61.
Cottet, G.-H., Koumoutsakos, P.D., 2000. Vortex Methods: Theory and Practice. Cambridge University Press.
Devenport, W.J., Rife, M.C., Liapis, S.I., Follin, G.J., 1996. The structure and development of a wing-tip vortex. J. Fluid Mech. 312, 67–106.
Feder, D.-F., Abdel-Maksoud, M., 2016a. Potential of the adaptive vorticity confinement method for RANS simulations and hybrid RANS-LES. In: Proceedings of the 7th International Conference on Vortex Flows and Vortex Models. Rostock, Germany.
Feder, D.-F., Abdel-Maksoud, M., 2016b. Tracking a tip vortex with adaptive vorticity confinement and hybrid RANS-LES. Open J. Fluid Mech. 6 (4).
Ferziger, J.H., Perić, M., 2002. Computational Methods for Fluid Dynamics, vol. 3. Springer, Berlin.
Gerz, T., Holzäpfel, F., Darracq, D., 2002. Commercial aircraft wake vortices. Prog. Aerosp. Sci. 38 (3), 181–208.
Gritskevich, M.S., Garbaruk, A.V., Schütze, J., Menter, F.R., 2012. Development of ddes and iddes formulations for the k-ω shear stress transport model. Flow Turbul. Combust. 88 (3), 431–449.
Hahn, S., Iaccarino, G., 2009. Towards adaptive vorticity confinement. In: 47th AIAA Aerospace Sciences Meeting Including the New Horizons Forum and Aerospace Exposition, Aerospace Sciences Meetings. AIAA.
Holzäpfel, F., Hofbauer, T., Darracq, D., Moet, H., Garnier, F., Gago, C.F., 2003. Analysis of wake vortex decay mechanisms in the atmosphere. Aerosp. Sci. Technol. 7 (4), 263–275.
Jasak, H., Tukovic, Z., June 2010. Dynamic mesh handling in openfoam applied to fluid-structure interaction simulations. In: Proceedings of the V European Conference Computational Fluid Dynamics, pp. 14–17. Lisbon, Portugal.
Jeong, J., Hussain, F., 1995. On the identification of a vortex. J. fluid Mech. 285, 69–94.
Kornev, N., 2016. Autowing Code Based on the Unsteady Nonlinear Vortex Lattice Method. http://www.lemos.uni-rostock.de/downloads/cfd/.
Kornev, N., Abbas, N., 2016. Numerical simulation of the tip vortex behind a wing oscillated with a small amplitude. J. Aircr. 54 (2). https://doi.org/10.2514/1.C033945.
Kornev, N., Matveev, K., 2003. Complex numerical modeling of dynamics and crashes of wing-in-ground vehicles. AIAA J. 600, 2003.
Launder, B.E., Reece, G.J., Rodi, W., 1975. Progress in the development of a Reynolds-stress turbulence closure. J. fluid Mech. 68 (3), 537–566.
Menter, F., Esch, T., 2001. Elements of industrial heat transfer predictions. In: 16th Brazilian Congress of Mechanical Engineering (COBEM), pp. 26–30.
Menter, F., Ferreira, J.C., Esch, T., Konno, B., Germany, A.C., 2003a. The SST turbulence model with improved wall treatment for heat transfer predictions in gas turbines. Proc. Int. Gas Turbine Congr. 2–7.
Menter, F., Kuntz, M., Langtry, R., 2003b. Ten years of industrial experience with the SST turbulence model. Turbul. heat mass Transf. 4 (1), 625–632.
Misaka, T., Holzäpfel, F., Gerz, T., 2013. Wake evolution of high-lift configuration from roll-up to vortex decay. AIAA Pap. 362 (2013), 11.
Nash'at, N.A., Proctor, F.H., Perry, R.B., 2013. Numerical simulation of the aircraft wake vortex flowfield. In: 5th AIAA Atmospheric and Space Environments Conference, American Institute of Aeronautics and Astronautics.
O'Regan, M., Griffin, P., Young, T., 2016. A vorticity confinement model applied to urans and les simulations of a wing-tip vortex in the near-field. Int. J. Heat Fluid Flow 61, 355–365.
Rozhdestvensky, K.V., 2006. Wing-in-ground effect vehicles. Prog. Aerosp. Sci. 42 (3), 211–283.
Samal, S.K., Shah, D.A., Bharath, M., Sahoo, A., 2013. Computational prediction of tip-vortex of a swept wing. Int. J. Innovat. Res. Sci. Eng. Technol. 2.
Shur, M.L., Spalart, P.R., Strelets, M.K., Travin, A.K., 2008. A hybrid RANS-LES approach with delayed-DES and wall-modelled LES capabilities. Int. J. Heat Fluid Flow 29 (6), 1638–1649.
Shur, M.L., Strelets, M.K., Travin, A.K., Spalart, P.R., 2000. Turbulence modeling in rotating and curved channels: assessing the spalart-shur correction. AIAA J. 38 (5), 784–792.
Smirnov, P.E., Menter, F.R., 2009. Sensitization of the SST turbulence model to rotation and curvature by applying the spalart–shur correction term. J. Turbomach. 131 (4).
Spalart, P.R., Allmaras, S.R., 1994. A one-equation turbulence model for aerodynamic Flows. La Recherche Aerospatiale 1.
Spalart, P.R., Deck, S., Shur, M., Squires, K., Strelets, M.K., Travin, A., 2006. A new version of detached-eddy simulation, resistant to ambiguous grid densities. Theor. Comput. Fluid Dyn. 20 (3), 181–195.
Steinhoff, J., Lynn, N., Wang, L., 2005. Computation of high reynolds number flows using vorticity confinement: I. Formulation. UTSI Preprint, University of Tennessee Space Institute.

Steinhoff, J., Underhill, D., 1994. Modification of the Euler equations for 'vorticity confinement': application to the computation of interacting vortex rings. Phys. Fluids 6 (8), 2738–2744.
Steinhoff, J., Yonghu, W., Mersch, T., Senge, H., 1992. Computational vorticity capturing: application to helicopter rotor flow. In: 30th Aerospace Sciences Meeting and Exhibit, Aerospace Sciences Meetings. AIAA.
Stephan, A., Holzäpfel, F., Misaka, T., 2014. Hybrid simulation of wake-vortex evolution during landing on flat terrain and with plate line. Int. J. Heat Fluid Flow 49, 18–27.
Weller, H.G., Tabor, G., Jasak, H., Fureby, C., 1998. A tensorial approach to computational continuum mechanics using object-oriented techniques. Comput. Phys. 12 (6), 620–631.
Wells, J., 2009. Effects of turbulence modeling on RANS simulations of tip vortices. Master's thesis. Virginia Polytechnic Institute and State University.
Wells, J., Salem-Said, A., Ragab, S.A., 2010. Effects of turbulence modeling on RANS simulations of tip vortices. In: 48th AIAA Aerospace Sciences Meeting Including the New Horizons Forum and Aerospace Exposition. Orlando, Florida.
Winckelmans, G., Leonard, A., 1993. Contributions to vortex particle methods for the computation of three dimensional incompressible unsteady ows. J. Comput. Phys. 109, 247–273.
Zhang, B., Lou, J., Kang, C.-W., Wilson, A., Lundberg, J., Svennberg, U., Bensow, R., et al., 2014. CFD modeling of propeller tip vortex over large distances. Int. J. Offshore Polar Eng. 24 (03), 181–183.